

# Distilled Low Rank Neural Radiance Field with Quantization for Light Field Compression

Jinglei Shi, Christine Guillemot, *Fellow, IEEE*

**Abstract**—In this paper, we propose a novel light field compression method based on a Quantized Distilled Low Rank Neural Radiance Field (QDLR-NeRF) representation. While existing compression methods encode the set of light field sub-aperture images, our proposed method instead learns an implicit scene representation in the form of a Neural Radiance Field (NeRF), which also enables view synthesis. For reducing its size, the model is first learned under a Low Rank (LR) constraint using a Tensor Train (TT) decomposition in an Alternating Direction Method of Multipliers (ADMM) optimization framework. To further reduce the model size, the components of the tensor train decomposition need to be quantized. However, performing the optimization of the NeRF model by simultaneously taking the low rank constraint and the rate-constrained weight quantization into consideration is challenging. To deal with this difficulty, we introduce a network distillation operation that separates the low rank approximation and the weight quantization in the network training. The information from the initial LR-constrained NeRF (LR-NeRF) is distilled to a model of a much smaller dimension (DLR-NeRF) based on the TT decomposition of the LR-NeRF. An optimized global codebook is then learned to quantize all TT components, producing the final QDLR-NeRF. Experimental results show that our proposed method yields better compression efficiency compared with state-of-the-art methods, and it additionally has the advantage of allowing the synthesis of any light field view with a high quality.

**Index Terms**—Light field, compression, low rank approximation, ADMM, network distillation, quantization.

## I. INTRODUCTION

**L**IGHT field imaging has gained in popularity due to its potential for computer vision or computational photography applications. However, light fields represent very large volumes of data, hence the need for compact representations and efficient compression algorithms. Many solutions have been designed for compressing light fields which encode the set of input views using either video compression techniques as HEVC or variants of this standard [1], [2]. Light field views are reordered as a pseudo video sequence (PVS) which is then fed into the video codec. A predefined scan order such as raster and spiral [3], [4] is typically used to generate a PVS. Approaches based on low rank models [5], [6] or 4D steered Gaussian mixture of experts [7] have also been proposed for light field compression. The Multidimensional Light field Encoder (MuLE) [8], which has been adopted in JPEG Pleno Coding standard as a transform-based coding approach, exploits the 4D redundancy of light field images by dividing them into 4D blocks. Thereafter, a 4D-DCT transform

is applied to the blocks to exploit the redundancy [9]. Similarly the use of 6D transforms is investigated in [10] for plenoptic point cloud compression. The authors in [11] describe a prediction method based on a Gaussian Process Regression technique applied on different classes of light field textures. Other methods consist in first synthesizing the entire light field from a subset of input views with the help of estimated disparity maps [12]–[15].

Here, we propose a completely different approach based on Neural Radiance Fields (NeRF) which have been recently introduced for scene representation and light field view synthesis [16]. NeRF is an implicit Multi-Layer Perceptron-based model that maps 5D vectors—3D coordinates plus 2D viewing directions—to opacity and color values, computed by fitting the model to a set of training views. The resulting neural model can then be used to generate any view of the light field using volume rendering techniques. Several variants have been proposed to reduce the number of input views as in [17], or to make the rendering more efficient [18]. A generalizable radiance field reconstruction is also proposed in [19] which can reconstruct radiance fields from only three nearby input views via fast network inference, and which can be used for rendering scenes different from those on which the network has been trained. An end-to-end framework, called NeRF-, is proposed in [20] for training NeRF models without pre-computed camera parameters. The authors in [21] consider more complex non-linear camera models and propose a new geometric loss function to jointly learn the geometry of the scene and the camera parameters. The authors in [22] generalize the usage of implicit neural representation to solve the problem of time, light and view interpolation.

NeRF can thus be seen as a neural representation of a scene which is learned from a set of input views. While existing light field compression solutions usually consider encoding and transmitting a subset of light field views which are then used at the decoder to synthesize and render the entire light field, we consider an alternative approach which optimizes and compresses the NeRF on the sender side, so that the network itself is transmitted to the receiver. The light field compression problem is thus cast into a problem of neural network compression. However, unlike compressing networks used in image classification or recognition tasks [23], compressing a view synthesis network is more challenging, due to the fact that the light field reconstruction quality is sensitive to network weight changes. The model should not only be compact, but should also preserve as much as possible high reconstruction quality.

In this paper, we first consider a simplified NeRF model

The authors are with Inria Rennes – Bretagne-Atlantique, 263 Avenue Général Leclerc, 35042 Rennes Cedex, France (e-mail: first-name.lastname@inria.fr).

based on only one MLP for rendering instead of the coarse and fine MLP in [16], which halves the number of parameters of the network. We optimize the network under a low rank constraint. The learning problem is formulated as a tensor rank optimization problem, solved using the Alternating Direction Method of Multipliers (ADMM) iterative optimization method. This low rank constraint allows us, following principles of network distillation [24], to transfer knowledge from this initial NeRF to a model of a much smaller dimension based on a Tensor Train (TT) decomposition. In other words, the weights of NeRF are decomposed into TT components using a distillation network, to decrease the number of parameters to be encoded. The TT parameters are further quantized using an optimized codebook. The knowledge transfer is made possible thanks to the low rank constrained optimization of the large NeRF model.

The performance in terms of compression efficiency of the proposed Quantized Distilled Low Rank Neural Radiance Field (QDLR-NeRF) for light fields has been assessed against the one obtained with a HEVC-based method [25], [26] and the Jpeg-pleno standard [27] in the 4D Prediction Mode. We also compare the obtained performances with those of recent deep learning video compression methods, in particular with the Hierarchical Learned Video Compression (HLVC) [28], the Recurrent Learned Video Compression (RLVC) [29] methods, and the OpenDVC [30] solution based on Deep Video Compression (DVC) [31]. These video compression methods are applied to the sequence of light field views. While achieving very good distortion-rate performance, such motion estimation-based deep compression networks, as well as similar methods such as in [32]–[35], often have complex structures, thus are not easy to train, and often need pre-trained optical flow estimators. Our experimental results show that our method outperforms very recent deep video compression methods requiring training on large datasets. It is also competitive against the standardized and highly optimized HEVC video compression tools applied to the sequence of views, as well as Jpeg-Pleno, a compression tool specifically designed for light fields.

So, in summary the contributions of this paper are:

- A low rank constrained simplified NeRF for compact light field representation.
- A network distillation operation that transfers knowledge from the LR-NeRF to a more compact scene light field representation model DLR-NeRF via Tensor Train decomposition.
- An efficient quantization operation guided by a global codebook, which tremendously reduces the total size of the representation with a limited distortion.
- A complete light field compression algorithm that integrates ADMM-based low rank optimization, network distillation and optimized quantization, giving superior performances when compared with light field reference compression methods.

Note that the proposed approach can be used beyond light field compression, in particular to reduce the memory footprint of NeRF, which can be critical for devices with low memory

resources.

## II. WORKFLOW AND NOTATIONS

We consider a light field represented by a 4D function  $L(x, y, u, v)$  [36], with  $(x, y) \in \llbracket 1, X \rrbracket \times \llbracket 1, Y \rrbracket$  and  $(u, v) \in \llbracket 1, U \rrbracket \times \llbracket 1, V \rrbracket$  respectively its angular and spatial coordinates.

The overall workflow of our method is shown in Fig. 1. The workflow is divided into three phases: 1) The low rank-constrained neural radiance field (LR-NeRF) optimization for scene reconstruction. 2) The network distillation for transferring knowledge from the LR-NeRF to a smaller model DLR-NeRF based on the Tensor Train decomposition. 3) The quantization of the TT components with an optimized codebook.

In the first step, a simplified NeRF with one MLP having weights  $\{W_i, b_i\}$  ( $i$  is the layer index) is trained as an implicit scene representation, with the goal of having the best scene reconstruction given the set of input views. The obtained NeRF is finetuned under a low rank constraint by applying Alternating Direction Method of Multipliers (ADMM) optimization. The tensor of the finetuned weights of LR-NeRF  $\{W_i^r, b_i\}$  becomes low-rank after this step, where  $r$  is the target rank. In the network distillation step, the weights of LR-NeRF are decomposed into a Tensor Train (TT) format as  $W_i^r = Q_i^1 \cdot Q_i^2$ , and we use  $\{Q_i^1, Q_i^2, b_i\}$  to initialize a distilled version of LR-NeRF noted DLR-NeRF. This step bonds the low rank optimization in previous step and the quantization in the next step. It can, on one hand, guarantee low rank property of  $W_i^r$ , on the other hand, allow quantifying  $Q_i^1, Q_i^2$  without degrading the final compression performance. The last quantization step aims at reducing the model size by quantifying the network weights. A global codebook  $C$  with  $N$  centroids is learned from  $Q_i^1, Q_i^2$  to quantify the values within the interval  $[-1, 1]$  of DLR-NeRF, from the first layer to the last layer gradually. Larger values outside the interval  $[-1, 1]$  are quantized with a uniform 16-bit quantizer. Thereafter, both sets of values inside and outside the interval  $[-1, 1]$  are coded using Huffman coding for optimal bitrate. The biases of the network  $b_i$  are converted to 16 bits for further compacting the model size. We denote the quantized weights of QDLR-NeRF as  $\{\hat{Q}_i^1, \hat{Q}_i^2, \hat{b}_i\}$

## III. METHOD

### A. Simplified Neural Radiance Field

In our method, we adopt NeRF to implicitly represent the scene, where 5D coordinates (location and view direction) of light rays  $(x, y, z, \theta, \phi)$  are fed into an MLP to produce a color and volume density  $(RGB, \sigma)$  for volumetric rendering. This procedure can be formulated as:

$$RGB, \sigma = F_{\Theta}(x, y, z, \theta, \phi), \quad (1)$$

with  $\Theta = \{W_i, b_i\}$  being weights and biases of the MLP.

Let us note that the original version of NeRF uses two MLPs to respectively coarsely and densely sample rays (i.e. performing a hierarchical volume sampling). The camera pose parameters are estimated from given views using the COLMAP structure-from-motion package [37]. We instead adopt one unique MLP for rendering, which halves the number

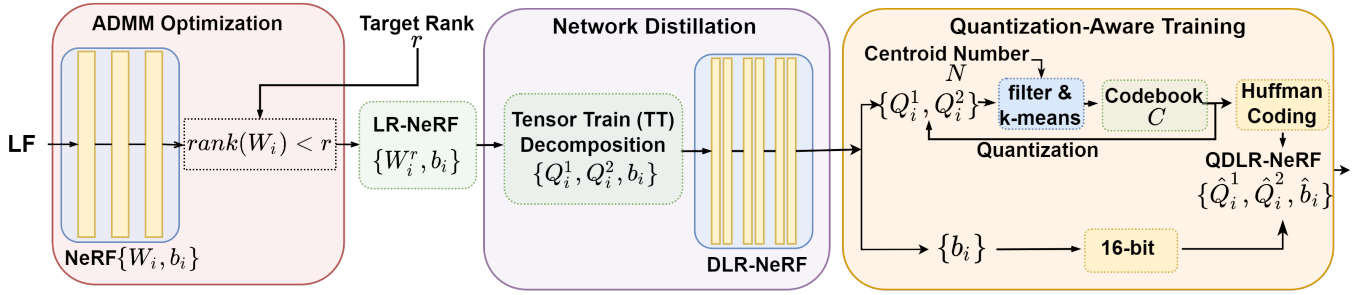


Fig. 1. Overall workflow of our proposed QDLR-NeRF method. A simplified NeRF (formed by only one MLP) is first trained from the set of input views, under a low rank (LR) constraint. The information from this LR-NeRF is distilled to a model of a much smaller dimension DLR-NeRF via the Tensor Train decomposition. The weight distillation is used to transfer knowledge in parameters of the large LR-NeRF to a smaller DLR-NeRF while keeping high performance. A codebook  $C$  with  $N$  centroids is learned to quantize DLR-NeRF to obtain the final compact QDLR-NeRF.

of parameters of the network. Since COLMAP may fail to estimate the camera pose parameters, especially for narrow-baseline light fields, we set the camera pose parameters as trainable parameters like in [20]. Focal length  $f$  and offset  $\Delta$  (proportional to the baseline) are the two camera pose parameters to be additionally optimized in our method (compared with unstructured views, the estimation of camera pose parameters of structured light fields is simpler). In this step, the rendering error is used as the loss function to supervise the initialization of NeRF and the update of its parameters  $\{W_i, b_i, f, \Delta\}$  as:

$$\operatorname{argmin}_{\{W_i, b_i, f, \Delta\}} \|c' - c_{gt}\|_2^2, \quad (2)$$

where  $c'$  is the rendered pixel value and  $c_{gt}$  is ground-truth pixel value.

### B. Low Rank NeRF approximation with ADMM

Although the initial NeRF [16] gives a good scene reconstruction and could be used for light field compression, its model size makes transmitting such a network less efficient than transmitting the compressed light field views. We therefore further reduce the model size by applying a TT decomposition [38] to the learned NeRF. The network weights  $W_i \in \mathbb{R}^{n_1 \times n_2}, \forall i$  are decomposed into the TT format as

$$W_i = Q_i^1 \cdot Q_i^2, \quad (3)$$

where  $Q_i^1 \in \mathbb{R}^{1 \times n_1 \times r}$  and  $Q_i^2 \in \mathbb{R}^{r \times n_2 \times 1}$  are the TT cores, and  $r$  is the target rank controlling the compression ratio. Straightforwardly decomposing the full-rank tensor  $W_i$  into a low-rank TT format inevitably causes a large approximation error, which degrades the light field reconstruction quality and the compression efficiency. To guarantee the low rank property of the tensor  $W_i$  without performance degradation, the authors in [39] formulate the model compression as a tensor rank optimization problem, and leverage Alternating Direction Method of Multipliers (ADMM) to solve this optimization problem in an iterative manner. In this section, we adopt this ADMM-based low rank approximation to finetune the learned NeRF. This optimization can be formulated as

$$\operatorname{argmin}_{\{W_i, b_i\}} \|c' - c_{gt}\|_2^2 \quad (4)$$

$$\text{s.t. } \operatorname{rank}(W_i) < r, \quad (5)$$

where  $r$  is the desired rank of  $W_i$ .

This non-convex optimization with constraints can be solved using the ADMM optimization method, after introducing an auxiliary variable  $Z$  and an indicator function  $g(\cdot)$ , as

$$g(W_i) = \begin{cases} 0, & \operatorname{rank}(W_i) < r \\ +\infty, & \text{otherwise.} \end{cases} \quad (6)$$

The original optimization problem can then be rewritten as:

$$\operatorname{argmin}_{\{W_i, Z_i\}} \|c' - c_{gt}\|_2^2 + g(Z_i) \quad (7)$$

$$\text{s.t. } W_i = Z_i \quad (8)$$

and the corresponding augmented Lagrangian in the scaled dual form of such an optimization problem is defined as

$$\mathcal{L}(W_i, Z_i, U_i) = l(W_i) + g(Z_i) + \frac{\rho}{2} \|W_i - Z_i + U_i\|_F^2 + \frac{\rho}{2} \|U_i\|_F^2, \quad (9)$$

where  $\rho$  is a positive penalty parameter,  $U_i$  is the dual multiplier, and  $l = \|c' - c_{gt}\|_2^2$  is the reconstruction error. The optimization of this Lagrangian term can be performed in an alternative way, as

$$W_i^{t+1} = \operatorname{argmin}_{\{W_i\}} \mathcal{L}(W_i^t, Z_i^t, U_i^t), \quad (10)$$

$$Z_i^{t+1} = \operatorname{argmin}_{\{Z_i\}} \mathcal{L}(W_i^{t+1}, Z_i^t, U_i^t), \quad (11)$$

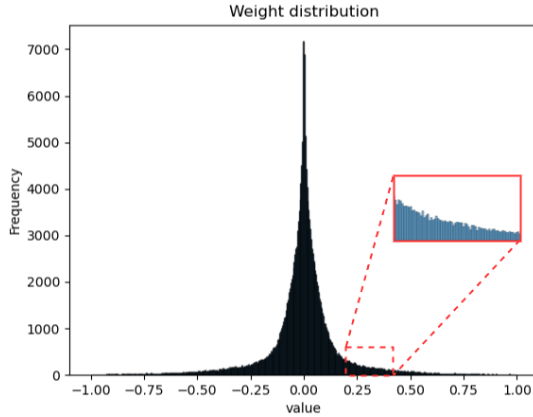
$$U_i^{t+1} = U_i^t + W_i^{t+1} - Z_i^{t+1} \quad (12)$$

Eq.10 corresponding to the updates of  $W_i$  can be solved using gradient descent. Eq.11 can be solved according to [40] as

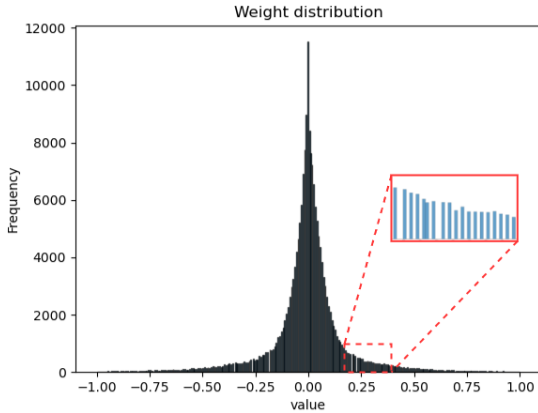
$$Z_i^{t+1} = \Pi_r(W_i^{t+1} + U_i^t), \quad (13)$$

where  $\Pi_r$  is the operation that decomposes the matrix into the TT format truncated to the desired rank  $r$ . One can refer to [39] for details on the ADMM procedure.

After this ADMM-based optimization procedure, the weights of the network  $W_i^r$  are low rank, hence can be decomposed into the TT format as in Eq. 3, with a small approximation error. For sake of simplicity, in the following, we neglect the first dimension of  $Q_i^1$  and the last dimension of  $Q_i^2$ , hence  $Q_i^1$  and  $Q_i^2$  are respectively with size  $n_1 \times r$  and  $r \times n_2$ . As the vector of bias parameters of each layer  $b_i$  is of rank 1, they are not considered in this optimization. In summary, after this low-rank optimization step, the parameters of the layers  $\{W_i^r, b_i\}$  are approximated by their TT components  $\{Q_i^1, Q_i^2, b_i\}$  for the following processing steps.



(a) Weight distribution before quantization



(b) Weight distribution after quantization, the number of centroid is 256.

Fig. 2. The weight distribution of  $\{Q_i^1, Q_i^2\}$  before&after rate-constrained quantization, we take light field scene ‘sideboard’ as an example, the target rank  $r = 40$  and number of centroid for quantization is  $N = 256$ .



Fig. 3. Reconstructed views (‘boxes(5,5)’) using (left) 16 bits quantization and (right) coarse quantization of the weights outside the interval  $[-1, 1]$ .

### C. Rate-Constrained Quantization

The decomposition of the weights  $W_i$  of the finetuned LR-NeRF into TT components reduces the model size. Beyond this low rank approximation, to further reduce the model size, one can in addition quantify the TT components  $\{Q_i^1, Q_i^2, b_i\}$  as follows.

We quantify  $\{Q_i^1, Q_i^2\}$  and  $\{b_i\}$  in different manners. As  $\{Q_i^1, Q_i^2\}$  occupy a much larger proportion of the total number of parameters, quantization is mainly performed on  $\{Q_i^1, Q_i^2\}$ . Fig. 2(a) shows the weight distribution of  $\{Q_i^1, Q_i^2\}, \forall i$ . One

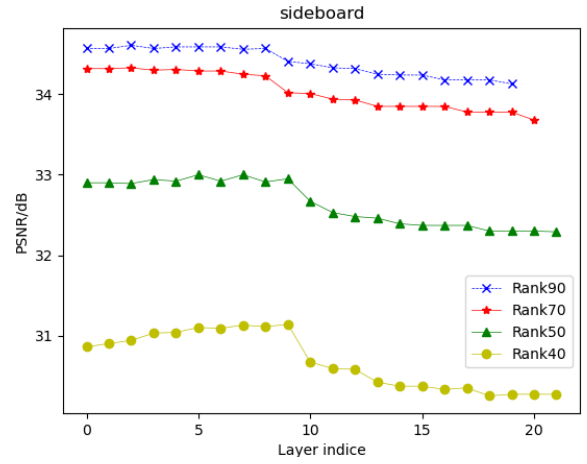


Fig. 4. PSNR evolution after quantizing each layer. We take the light field scene ‘sideboard’ with different ranks  $r = \{40, 50, 70, 90\}$  as an example.

can observe that most of the parameters are within the interval  $[-1, 1]$ . Quite few parameters are outside the interval  $[-1, 1]$ . These parameters represent about 0.5% of the total number of parameters of  $\{Q_i^1, Q_i^2\}$ . However, as we show in Fig. 3, the weights outside the interval  $[-1, 1]$  are essential to have a good light field reconstruction and should not be coarsely quantized, which explains our choice of using a fine 16 bit quantizers for these low probability values.

Therefore we quantize the weights inside and outside the interval  $[-1, 1]$  in two different manners. More specifically, the weights outside  $[-1, 1]$  are quantized using a uniform 16 bits quantizer to keep enough precision. In contrary, the weights within  $[-1, 1]$  are quantized using a non uniform optimized quantizer, whose codebook  $C$  is obtained by applying the k-means method to cluster weights into  $N$  centroids. This is motivated by the fact that the two sets of weights have very different distributions. The weights outside the interval  $[-1, 1]$  have a low and close to uniform probability, making the use of a k-means based optimized quantizer less relevant for this set of weights. In addition, the low number of values would make the clustering, hence the quantization, not very effective.

Unlike in [41], where the authors learn a codebook for each layer of the network, we learn a unique codebook  $C$  to quantize the weights within  $[-1, 1]$  in all layers. Fig. 2(b) shows the weight distribution after rate-constrained quantization with 256 centroids. To alleviate the performance loss caused by this quantization, we adopt a quantization-aware training strategy in this step, i.e., after quantizing  $\{Q_n^1, Q_n^2\}$  of layer  $n$ , we continue to train the other layers and update  $\{Q_i^1, Q_i^2\} \forall i > n$  and  $\{b_i\} \forall i$ . Once all layers have been quantized, we update the codebook and proceed with a new quantization. In our experiment, we however found that, in most of cases, only one round of codebook update is enough. We show in Fig. 4 the performance loss after quantizing layers from the first to the last, one can notice that thanks to our quantization-aware training procedure, there is barely any PSNR loss after quantizing first several layers, performance degradation is mainly caused by quantization of some layers and is quite limited. When the weights of all the layers have been quantized, we losslessly

encode them using Huffman Coding. While we could encode separately the two sets of weights, we instead construct a Huffman code table for all the values (within and outside the interval  $[-1, 1]$ ). Separately encoding each set with an entropy code (e.g. Huffman code) would require sending an extra flag to signal whether the weight belongs to one set or the other, which would penalize the entire bit rate. Even if having a unique Huffman codebook for a larger number of weight values (the union of the two sets) would in theory increase the average Huffman code length, the number of large value is sufficiently small so that this average code length is not significantly increased. Simulations have shown that this solution was indeed more efficient in terms of bitrate. Biases  $\{b_i\}$  are simply saved using 16 bits.

One could think of integrating both constraints of low rank approximation and weight quantization within the ADMM framework. However, this is extremely challenging. Indeed, since the low rank tensor approximation and the weight quantization are not convex functions, their integration in the ADMM framework may raise convergence issues.

Another option is to consecutively apply these two techniques, i.e., finetuning the network with a low rank constraint (getting  $W_i^r$ ), then decomposing  $W_i^r$  into TT components and quantizing them (getting  $\hat{Q}_i^1$  and  $\hat{Q}_i^2$ ) finally retrieving the weights  $\hat{W}_i^r$ . Although this option avoids considering low rank constraint and quantization at the same time in ADMM, due to the fact that the quantization operation is performed on TT components  $Q_i^1, Q_i^2$  instead of  $W_i$  itself, any subtle perturbation on  $Q_i^1, Q_i^2$  may lead to significant variations of the weights  $W_i^r$ . Hence such an option is unstable and the light fields reconstructed using  $\hat{W}_i^r$  are prone to artifacts.

In order to avoid the above difficulties, and better bond the low rank optimization and the quantization of the TT components, we propose a ‘distilled’ version of LR-NeRF. More specifically, for weights and bias  $\{W_i^r, b_i\}$  in each layer of LR-NeRF, we use the corresponding TT components  $Q_i^1, Q_i^2$  and bias  $b_i$  to initialize two distilled layers, which finally gives us a distilled architecture.

#### D. Network Distillation

The distillation of LR-NeRF is crucial to our workflow, since it leads to a smaller network whose weights are defined by the matrices  $Q_i^1$  and  $Q_i^2$ . This distillation mechanism also allows quantizing  $Q_i^1$  and  $Q_i^2$  without necessity to reconstruct  $W_i^r$ , as  $Q_i^1$  and  $Q_i^2$  are the weights of the smaller distilled network. Therefore the low-rank constrained ADMM optimization in the first step and quantization-aware training in the last step are ‘physically’ separated by this network distillation. The rank optimization and the bitrate optimization will not mutually interfere.

Please note that a layer with weight  $W_i^r$  is actually distilled into two layers with weights  $Q_i^1$  and  $Q_i^2$  only if the resulting number of parameters is reduced compared to the number of weight values in the matrix  $W_i^r$ .

We further train DLR-NeRF for a certain number of epochs after initializing it using  $Q_i^1, Q_i^2, b_i$ . Please note that one could also skip the previous NeRF initialization and low rank

finetuning procedures, and train a distilled NeRF from scratch. However, as we will discussed in Sec. V-C1, the weights trained from scratch follow a different distribution from the one of the low-rank weights, and they fail to reconstruct high quality scene views.

After applying the quantization operation on this DLR-NeRF, the obtained QDLR-NeRF can be used to represent a light field in the compression context. One can indeed transmit the quantized network weights  $\hat{Q}_i^1, \hat{Q}_i^2$  (after Huffman Coding),  $\hat{b}_i$  (16 bits), the codewords (32 bits) and the camera parameters  $f, \Delta$  (32 bits) from the sender to the receiver.

#### IV. TRAINING SCHEDULE AND HYPERPARAMETERS

The training of such a workflow has four phases, as follows.

a). **Training the simplified NeRF:** We simplified the architecture of NeRF by adopting one single MLP for inference. The depth of the adopted MLP is 8 and the number of channels is 256. We set the sampling rate along the rays to 128 and the camera pose parameters  $(f, \Delta)$  are initialized to  $f = 0.01W$  ( $W$  is the width of the light field views),  $\Delta = 10$ . We adopt normalized depth for rendering. When training such a network, we followed the default configuration in [16], with the initial learning rate set to  $5 \times 10^{-4}$  and the exponential decay rate to 0.1. We finally trained the network for  $3 \times 10^5$  iterations.

b). **Finetuning LR-NeRF:** We finetuned LR-NeRF following the same configuration as in the previous step, except that in this step, the camera pose parameters are no longer updated. We finetune LR-NeRF for  $3 \times 10^5$  iterations. The penalty factor  $\rho$  for ADMM is set to 10.

c). **Finetuning DLR-NeRF:** After the TT decomposition of the LR-NeRF weights and the initialization of DLR-NeRF, we continued to finetune DLR-NeRF for  $2 \times 10^5$  iterations, during which the camera pose parameters are kept fixed.

d). **Quantizing DLR-NeRF:** The quantization of the layers of DLR-NeRF is gradually carried out from the first to the last layer. After quantizing each layer, we train the other layers for  $3 \times 10^4$  iterations. The initial codebook for the interval  $[-1, 1]$  is obtained after 20 iterations of clustering in the k-means algorithm. Although the codebook can be updated after each round of quantization, we just update it once in practice. Our proposed workflow has been implemented using pytorch and has been trained on a GPU of type GeForce RTX 2080 Ti with 11 GB memory.

#### V. COMPRESSION PERFORMANCE ANALYSIS

##### A. Settings

We first trained a simplified NeRF with full rank. This initial model is then finetuned and distilled using four different ranks  $r = \{150, 90, 70, 40\}$ , and we finally quantized the distilled models with  $N = 256$  centroids. The quantized models having a lower rank have fewer parameters, hence give a lower bitrate. We found that, when the target rank  $r$  is lower than 40, the light field reconstructed with the distilled Low-Rank NeRF (DLR-NeRF) is prone to artifacts. Therefore, we do not decrease the rank below 40, and to decrease the bitrate, we reduce the number of centroids to further reduce the model size. More precisely, we set  $N = \{256, 64, 32\}$  when  $r = 40$ .

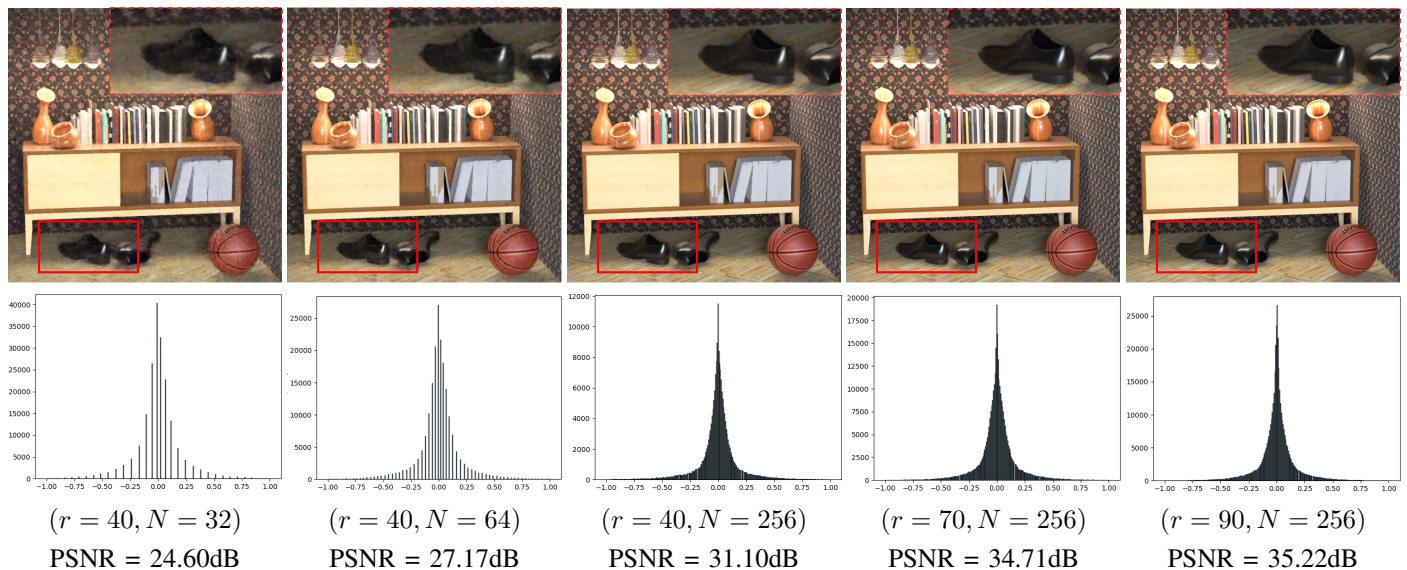


Fig. 5. We show in the first row the central view of the light field ‘sideboard’ reconstructed by quantized DLR-NeRF with different rank&centroid settings. The second row shows the weight distribution of each quantized DLR-NeRF. Larger is the rank of the model and higher is the number of centroids, better will be the reconstructed view.

To test the effectiveness of our method, we carry out experiments using both synthetic and real-world light fields. Both of them are from widely used light field benchmark. For synthetic light fields, we took four scenes *boxes*, *sideboard*, *cotton*, *dino* from the HCI dataset [42], each of them has an angular resolution  $(U, V) = (9, 9)$  and a spatial resolution  $(X, Y) = (512, 512)$ . While for real-world light fields, we took four scenes *Bikes*, *Danger*, *StonePillarsOutside*, *FountainVincent2* from the EPFL light field dataset [43], which have been captured using a plenoptic Lytro Illum camera. We took the central  $9 \times 9$  views, each view having a spatial resolution of  $432 \times 624$ . Although ground truth camera poses are already available for synthetic data, we estimated the camera poses for both the synthetic and real-world data to show that our workflow is not limited by the availability of the camera pose parameters.

### B. Rate-Distortion Performance

Fig. 5 shows the central view reconstructed using the QDLR-NeRF with different  $(r, N)$  settings, and their corresponding weight probability distributions. One can easily notice that, larger is the rank of the DLR-NeRF model or higher is the number of centroids better is the reconstructed view. This is quite intuitive, as a larger rank means more parameters a model has, and more centroid means less quantization noise.

However, in the compression context, besides the quality of the ‘compressed views’, we also need to take bitrate into account, i.e. the rate-distortion performance. To investigate the compression performance of our proposed method, we measure the rate-distortion performances with different rank&centroid settings, and compare them with those obtained when applying State-Of-The-Art (SOTA) video compression methods to light fields, by encoding the views as a pseudo video sequence. The codecs that we consider are the HEVC-Lozenge [44], the Jpeg-pleno VM2.0 standard designed specif-

ically for light field compression, and learning-based RLVC [29], HLVC [28] and OpenDVC [30] compression methods. OpenDVC is an open implementation of the DVC [31].

For the settings of each reference method, we use the HEVC HM-16.10 implementation in our test, with a GOP size equal to 4. The Jpeg-pleno standard needs an input disparity map that we estimated using the technique in [45]. When considering the RLVC, HLVC and OpenDVC methods, we directly used the authors’ codes with the recommended configurations, i.e., for the RLVC method, we set the P-frames number to 6 for both the forward and backward directions, which means a GOP size of 13, while for the HLVC and OpenDVC methods, we used the default setting of GOP size equal to 10. When testing the reference methods RLVC, HLVC and OpenDVC, we used their trained models. There are four pre-trained models for each method, with an optional hyper-parameter  $\lambda = \{256, 512, 1024, 2048\}$  that controls the trade-off between distortion and bitrate. Higher  $\lambda$  means less distortion but larger bitrate.

Fig. 6 shows the PSNR-Rate curves of each method with different light fields. The bitrate is evaluated by bit per pixel (bpp). One can observe from the figures, that our proposed method outperforms the reference methods on synthetic data at moderate bitrate by a margin about 1dB in most of the tested scenes. While on real-world light fields, though the margin is smaller than that of synthetic data, our method still shows superiority than other referenced methods in most of cases. Actually, due to the fact that light fields captured by Lytro Illum may contain artifacts such as vignetting, blurriness etc., which are caused by its hardware. When applying a NeRF-based compression method, these artifacts will prevent our method from reconstructing the accurate scene, hence lowering the PSNR of the reconstructed views.

Figure 7 shows the averaged error maps for the different methods. Note that the error maps are averaged over all the

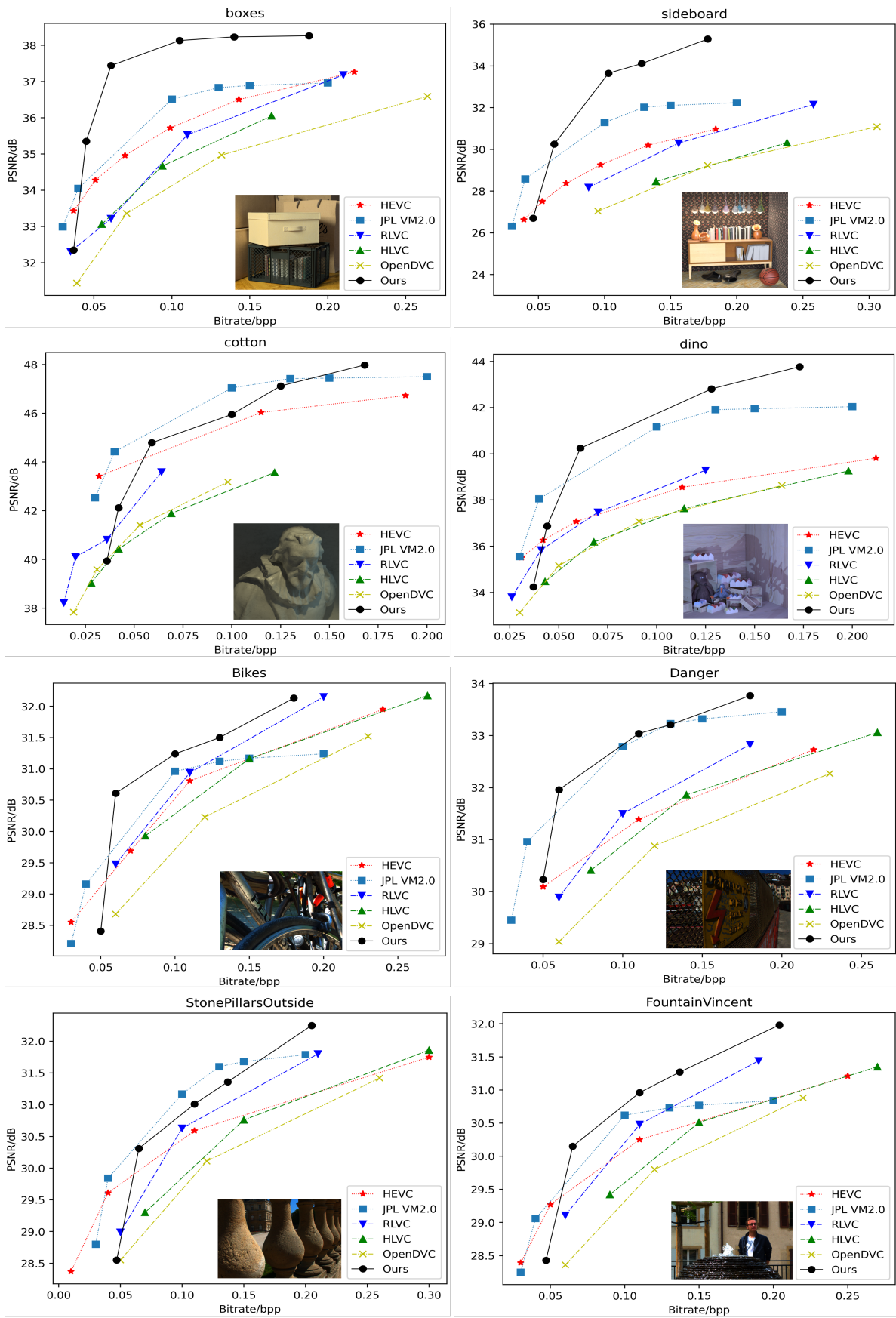


Fig. 6. Rate-distortion curves of different compression methods, with tested light fields from the HCI synthetic dataset [42] and the EPFL real-world dataset [43].

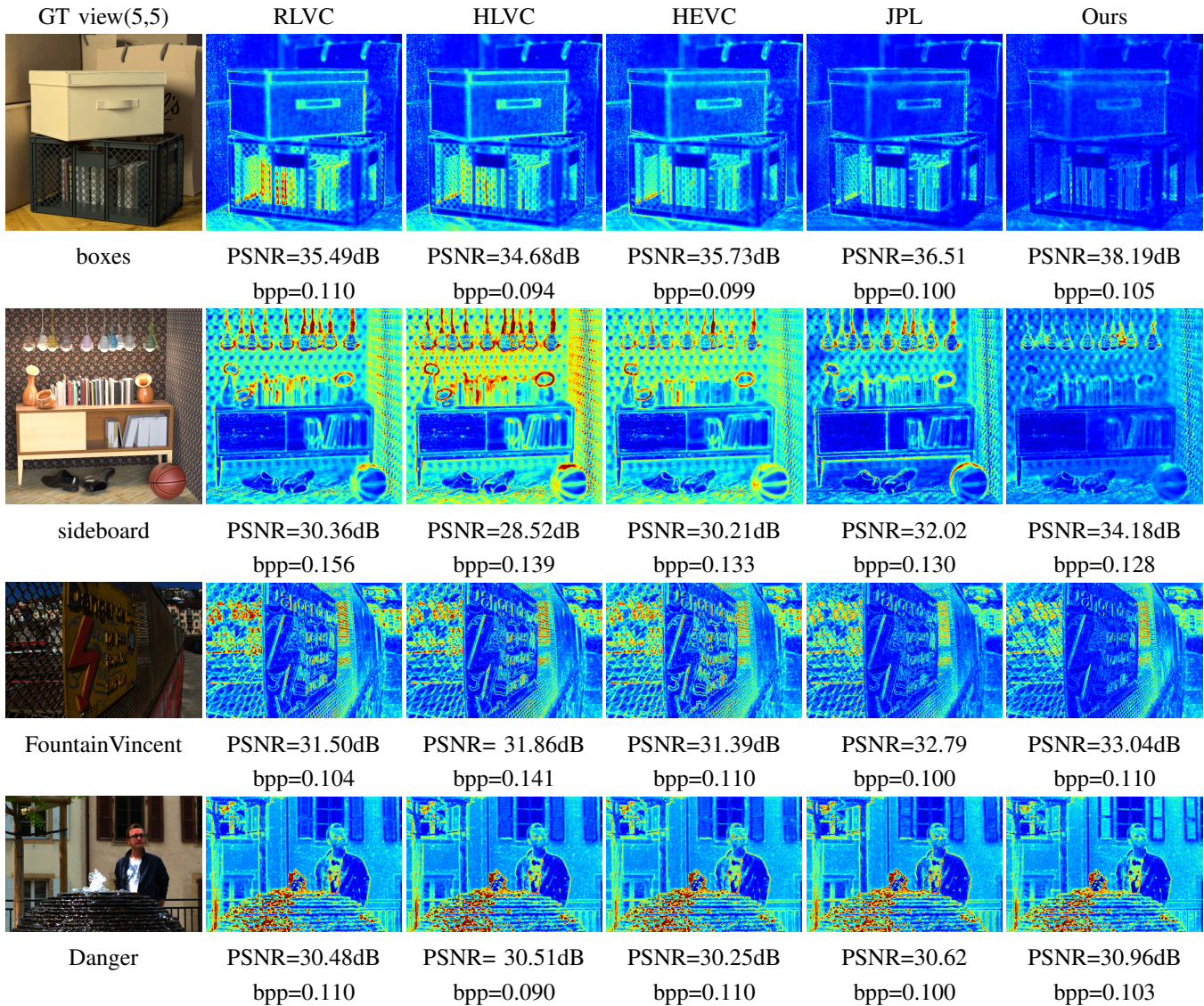


Fig. 7. Averaged reconstruction error maps of decompressed light fields, when using the RLVC, HLVC, HEVC, Jpeg-pleno methods and our method, along with the corresponding PSNR and bitrate values.

views, to account for the fact that some methods, such as Jpeg-Pleno, RLVC, OpenDVC, lead to strong variations in quality on the different views (see Fig. 8). We can observe that our method yields lower error and better compression results than other methods on synthetic data (*boxes*, *sideboard*). When using real-world Lytro light fields suffering from color inconsistency between angular views, our method may learn inaccurate scene information and hence generate some errors (like the windows in scene *FountainVincent*). However, it can still well capture scene geometry information and better reconstruct the object contours (like the contours of the person in the scene).

Compared with the referenced methods that compress each input frame, our method focuses on retrieving the entire scene with as fewer parameters as possible. This distinct design endows our method with two advantages:

1). Better consistency across views. Fig. 8 shows the PSNR variations in terms of viewpoints (For Jpeg-pleno, the central

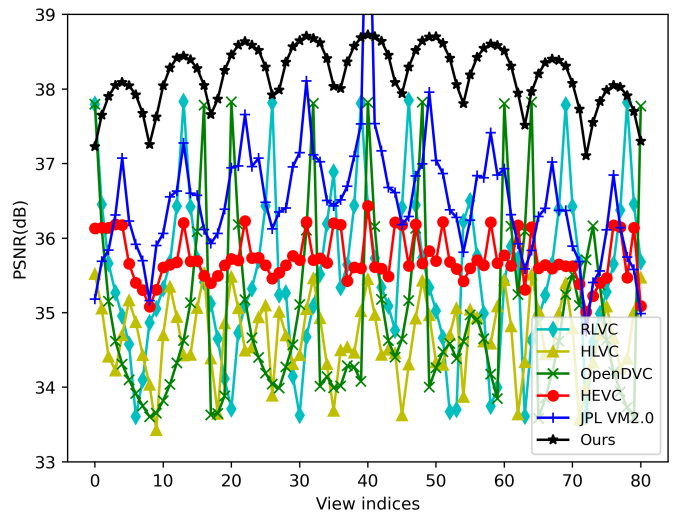


Fig. 8. PSNR variation along the viewpoints for the light field ‘boxes’. All views have been compressed at a similar bitrate.

view serves as the reference view and has higher PSNR). Similarly, the RLVC, DLVC and OpenDVC methods first intra code key frames, and then compress the other frames within the GOP using motion-compensated inter-coding. The quality of the compressed light fields is therefore not stable and varies across the different viewpoints. In contrast, our method yields views with a more consistent quality and higher PSNR values. Each view is indeed rendered independently, thus enabling full random access, which is not the case of methods relying on inter-coding.

2). Capacity of rendering views in any angular position. Different from other methods that compress a set of input views, our method, thanks to NeRF, encodes the scene information. Hence the scene can be flexibly reconstructed by rendering the light field in any angular position on the decoder side.

### C. Ablation Study

In this section, we evaluate different aspects of the proposed method.

1) *Random initialization vs Low-rank initialization*: As aforementioned in Sec. III-D, instead of the proposed NeRF initialization and finetuning steps, one could directly train a distilled NeRF with randomly initialized weights. Although this variant has a simpler training schedule, we show that it severely degrades the quality of the reconstruction. To evaluate the interest of the proposed distillation approach, we adopted the architecture of the distilled NeRF with rank 40, and respectively initialized it using random weights (noted as NeRF-rand) and low-rank weights (noted as NeRF-lr). We then trained the two models until convergence. To guarantee the same experimental conditions, the two variants share the same camera pose and are trained without quantization. Table I shows the PSNR of the light fields generated by NeRF-rand and NeRF-lr, with the same camera pose. The distilled NeRF trained with randomly initialized weights yields poor reconstruction quality. While NeRF trained with low-rank weights gives a good reconstruction quality. Fig. 9 shows views reconstructed when using the two variants, and an example of weight distribution (for the light field ‘boxes’). From the figure, we can observe that the weights of NeRF-rand and NeRF-lr follow different distributions. NeRF-lr has more values around 0 and long tails, NeRF-rand has fewer values around 0. Most weights are within the interval  $[-0.25, 0.25]$  and the distribution does not have long tails. In terms of reconstruction quality, NeRF-rand produces views with severe blurriness, while NeRF-lr gives views with subtle details, which means that it is better to use the low-rank NeRF to initialize the distilled version. The difference in terms of performance between NeRF-lr and NeRF-rand can be explained by the fact that, due to its low number of parameters of the distilled network, the optimization of the distilled network from scratch (with random initialization) may fall in local minima, giving a lower performance compared to the use of weights resulting from the low rank approximation of the large network.

2) *Quantization strategy analysis: Local quantization vs global quantization* Instead of using a global codebook of

Variants	boxes	sideboard	dino	cotton	average
NeRF-rand	25.18dB	19.88dB	23.27dB	32.56dB	<b>25.22dB</b>
NeRF-lr	37.85dB	30.93dB	40.90dB	45.18dB	<b>38.72dB</b>

TABLE I  
AVERAGE PSNR OF VIEWS GENERATED BY NeRF INITIALIZED WITH RANDOM WEIGHTS AND WITH LOW-RANK WEIGHTS (WITH  $r = 40$ ). BOTH VARIANTS HAVE FULLY CONVERGED.

Quantization options	PSNR	Bitrate
DLR-NeRF-noQuant	38.72dB	0.30bpp
DLR-NeRF-localQuant	38.70dB	0.12bpp
DLR-NeRF-globalQuant	38.18dB	0.06bpp

TABLE II  
AVERAGE PSNR AND BITRATE OBTAINED WHEN USING DIFFERENT QUANTIZATION OPTIONS: WITH NO QUANTIZATION (DLR-NeRF-NOQUANT), WITH ONE CODEBOOK FOR EACH LAYER (DLR-NeRF-LOCALQUANT), AND WHEN USING A SHARED CODEBOOK FOR ALL LAYERS (DLR-NeRF-GLOBALQUANT).

$N$  centroids for quantizing all layers, one can also utilize one codebook optimized for each layer. Table II shows the average PSNR and bitrate obtained when using the different quantization options, i.e. with no quantization (DLR-NeRF-noQuant), with a quantizer optimized for each layer (DLR-NeRF-localQuant) and a global codebook for all layers (DLR-NeRF-globalQuant). The local quantization suffers less from distortion but increases significantly the bitrate compared with the global quantization. While global quantization brings more distortion, its compression ratio is higher. Therefore, we adopted a global quantizer as it gives a lower bitrate with acceptable performance loss. Moreover, learning one codebook is much easier than learning several codebooks per layer.

3) *Contribution of the different blocks of the architecture*: To justify the contribution of each building block of the workflow, we measure the averaged PSNR and the model size after each step of our algorithm, and set original NeRF [16] (NeRF-org) as our baseline, with whose size being 100%. The original NeRF has coarse and fine MLPs, and uses ground truth camera poses for synthesis. In our workflow, we instead adopt a simplified NeRF with only one MLP to learn scene information, and optimize it with a low rank constraint (LR-NeRF). The camera poses are estimated during the optimization of the LR-NeRF. Then this LR-NeRF is distilled into the DLR-NeRF with respect to the desired rank, here, we set desired the rank to  $r = 40$  for LR-NeRF and DLR-NeRF. DLR-NeRF is finally quantized with the number of centroids set to  $N = 256$  to obtain QDLR-NeRF.

Table III gives the PSNR and the model size evolution after each step of our workflow. The PSNR and size values are averaged over four synthetic scenes. We can observe from the table that, the transition from NeRF-org to LR-NeRF brings about 3dB PSNR loss. The loss is due to two factors: 1.) The camera poses are estimated instead of being ground truth camera poses, which introduces some errors 2.) The low rank constraint slightly decreases the synthesis performance. One could also think that this loss is caused by using only one MLP for synthesis. However, with most of light fields, the default sampling rate of 128 along light rays is enough for one single



Fig. 9. Weight distribution and views reconstructed using NeRF-rand (1st row) and NeRF-lr (2nd row), with several scenes.

Metrics	NeRF-org	LR-NeRF	DLR-NeRF	QDLR-NeRF
PSNR	41.98dB	38.83dB	38.72dB	38.18dB
Size	100%	50%	16.7%	3.3%

TABLE III

PSNR AVERAGED ON THE 8 TEST LIGHT FIELDS AT THE DIFFERENT STEPS OF THE PROPOSED WORKFLOW: ORIGINAL NERF (NeRF-ORG), NERF WITH THE LOW RANK CONSTRAINT (LR-NeRF), DISTILLED LOW-RANK NERF (DLR-NeRF) AND AFTER QUANTIZATION OF DLR-NeRF (QDLR-NeRF).

MLP to yield high quality reconstruction. The replacement of two MLPs by one barely bring any performance loss.

From LR-NeRF to DLR-NeRF, by distilling the network with the desired rank  $r = 40$ , we reduce the model size by a factor of 3 with only a 0.1dB PSNR loss. This small loss means, that the target rank of 40 (the full rank being 256) can already store most of scene information for reconstruction, which also proves the effectiveness of our low rank approximation. From DLR-NeRF to QDLR-NeRF, the network is quantized from the first to the last layer, this gradual quantization step effectively reduces the model size to 1/5, with a limited performance loss of 0.6dB. In summary, thanks to the proposed low rank optimization, network distillation and quantization operations, we ultimately reduce the model size from 100% (the reference being the bit number of the original NeRF) to 3.3%, which is crucial in a context of light field compression, but also simply in terms of storage requirement for the NeRF model.

## VI. DISCUSSION

Although our proposed method is able to effectively compress light fields, due to the fact that, it is based on the NeRF method, factors that limit the performance of NeRF will consequently become limitations of our method. For example, when applying NeRF to learn light fields captured by Lytro, blurriness and vignetting in each sub-aperture view may

prevent the network from reconstructing precise scenes. As a result, the compression performance of our QDLR-NeRF is limited by these artifacts. While better performance is obtained on synthetic data, as they do not include these artifacts. That also explains why the gaps between the rate-distortion curves of our method and those of the reference methods on synthetic light fields are larger than those on Lytro-captured light fields.

Finally, please note that, even if we have chosen the original NeRF to demonstrate the interest of the proposed method, the method can obviously apply to different variants of NeRF implementations, e.g., SIREN [46], PlenOctrees [47], including to the recent SIGNET solution [48].

## VII. CONCLUSION

In this paper, we have proposed a Quantized Distilled Low Rank Neural Radiance Field (QDLR-NeRF) representation for light field compression. The method optimizes a NeRF with a low rank constraint using an ADMM optimization framework to obtain the so-called LR-NeRF, the weights in LR-NeRF are low-rank, hence can be decomposed into a Tensor Train format. The decomposed weights are then used to initialize a distilled version of NeRF named DLR-NeRF, which has fewer parameters. Finally, we gradually quantize the layers of DLR-NeRF from the first layer to the last one using a global codebook learned by k-means, to get QDLR-NeRF. The distillation operation avoids tackling the rank-constrained optimization and the rate-constrained quantization simultaneously, making the entire pipeline work stably to compress a light field. The low rank optimization and quantization operations effectively reduce the size of the model without significantly degrading the reconstruction performance. Experimental results, using both synthetic and real-world light fields, show that our method outperforms the reference methods with a large margin. Furthermore, due to the fact that our method is based on synthesis method, it also has the advantage of generating novel views as densely as possible.

## ACKNOWLEDGMENT

This work was supported in part by the french ANR research agency in the context of the artificial intelligence project DeepCIM, and in part by the EU H2020 Research and Innovation Programme under grant agreement No 694122 (ERC advanced grant CLIM). We would also like to show our gratitude to Prof. Zhaolin Xiao, Dr. Xi Wang and Mr. Kai Gu for inspiring discussions.

## REFERENCES

- [1] C. Conti, P. Nunes, and L. Soares, "HEVC-based light field image coding with bi-predicted self-similarity compensation," in *IEEE Int. Conf. on Multimedia Expo. Workshops (ICMEW)*, 2016, pp. 1–4.
- [2] W. Ahmad, M. Ghafoor, S. A. Tariq, A. Hassan, M. Sjöström, and R. Olsson, "Computationally efficient light field image compression using a multiview HEVC framework," *IEEE Access*, vol. 7, 2019.
- [3] F. Dai, J. Zhang, Y. Ma, and Y. Zhang, "Lenselet image compression scheme based on subaperture images streaming," in *IEEE Int. Conf. on Image Processing (ICIP)*, 2015, pp. 4733–4737.
- [4] H. Amirpour, M. Pereira, and A. Pinheiro, "High efficient snake order pseudo-sequence based light field image compression," in *IEEE Data Compression Conf. (DCC)*, 2018, pp. 397–397.
- [5] E. Dib, M. L. Pendu, and C. Guillemot, "Light field compression using fourier disparity layers," in *IEEE Int. Conf. on Image Processing (ICIP)*, 2019, pp. 3751–3755.
- [6] X. Jiang, M. L. Pendu, R. Farrugia, and C. Guillemot, "Light field compression with homography-based low-rank approximation," *IEEE J. Sel. Topics Signal Process. (JSTSP)*, vol. 11, no. 7, pp. 1132–1145, Oct. 2017.
- [7] R. Verhack, T. Sikora, G. V. Wallendaal, and P. Lambert, "Steered mixture-of-experts for light field images and video: Representation and coding," *IEEE Trans. on Multimedia (TMM)*, vol. 22, no. 3, pp. 579–593, 2020.
- [8] M. de Carvalho, M. Pereira, G. Alves, E. da Silva, C. Pagliari, F. Pereira, and V. Testoni, "A 4D DCT-based lenslet light field codec," in *IEEE Int. Conf. on Image Processing (ICIP)*, 2018, pp. 435–439.
- [9] M. Magnor, A. Endmann, and B. Girod, "Progressive compression and rendering of light fields," *Conf. on Vision, Modeling & Visualization (VMV)*, 2000.
- [10] M. Krivokuca, E. Mianjji, C. Guillemot, and P. Chou, "Compression of plenoptic point cloud attributes using 6-d point clouds and 6-d transforms," *IEEE Trans. on Multimedia (TMM)*, 2021.
- [11] D. Liu, P. An, R. Ma, W. Zhan, X. Huang, and A. Yahya, "Content-based light field image compression method with gaussian process regression," *IEEE Trans. on Multimedia (TMM)*, vol. 22, no. 4, pp. 846–859, 2019.
- [12] W. Ahmad, S. Vagharshakyan, M. Sjöström, A. Gotchev, R. Gregovic, and R. Olsson, "Shearlet transform based prediction scheme for light field compression," in *Data Compression Conf. (DCC)*, 2018, pp. 396–396.
- [13] X. Jiang, M. L. Pendu, and C. Guillemot, "Light field compression using depth image based view synthesis," in *IEEE Int. Conf. on Multimedia Expo Workshops (ICMEW)*, 2017, pp. 19–24.
- [14] Y. Zhang, W. Dai, Y. Li, C. Li, J. Hou, J. Zou, and H. Xiong, "Light field compression with graph learning and dictionary-guided sparse coding," *IEEE Trans. on Multimedia (TMM)*, 2022.
- [15] X. Huang, P. An, Y. Chen, D. Liu, and L. Shen, "Low bitrate light field compression with geometry and content consistency," *IEEE Trans. on Multimedia (TMM)*, vol. 24, pp. 152–165, 2022.
- [16] B. Mildenhall, P. Srinivasan, M. Tancik, J. Barron, R. Ramamoorthi, and R. Ng, "NeRF: Representing scenes as neural radiance fields for view synthesis," in *Eur. Conf. on Computer Vision (ECCV)*, 2020, pp. 405–421.
- [17] A. Yu, V. Ye, M. Tancik, and A. Kanazawa, "pixelNeRF: Neural radiance fields from one or few images," *IEEE Int. Conf. on Computer Vision and Pattern Recognition (CVPR)*, pp. 4576–4585, 2021.
- [18] L. Liu, J. Gu, K. Lin, T. Chua, and C. Theobalt, "Neural sparse voxel fields," *Advances in Neural Information Processing Systems (NIPS)*, 2020.
- [19] A. Chen, Z. Xu, F. Zhao, X. Zhang, F. Xiang, J. Yu, and H. Su, "MVSNerF: Fast generalizable radiance field reconstruction from multi-view stereo," in *IEEE Int. Conf. on Computer Vision (ICCV)*, 2021.
- [20] Z. Wang, S. Wu, W. Xie, M. Chen, and V. Prisacariu, "NeRF—: Neural radiance fields without known camera parameters," *arXiv preprint arXiv:2102.07064*, 2021.
- [21] Y. Jeong, S. Ahn, C. Choy, A. Anandkumar, M. Cho, and J. Park, "Self-calibrating neural radiance fields," in *IEEE Int. Conf. on Computer Vision (ICCV)*, 2021, pp. 5846–5854.
- [22] M. Bemana, K. Myszkowski, H. Seidel, and T. Ritschel, "X-Fields: Implicit neural view-, light- and time-image interpolation," *ACM Trans. on Graphics (TOG)*, vol. 39, no. 6, 2020.
- [23] S. Han, H. Mao, and W. J. Dally, "Deep compression: Compressing deep neural networks with pruning, trained quantization and Huffman coding," *Int. Conf. on Learning Representations (ICLR)*, 2016.
- [24] G. Hinton, O. Vinyals, and J. Dean, "Distilling the knowledge in a neural network," *ArXiv*, vol. abs/1503.02531, 2015.
- [25] G. Sullivan, J. Ohm, W. Han, and T. Wiegand, "Overview of the high efficiency video coding (HEVC) standard," *IEEE Trans. Circuits Syst. Video Technol. (TCSVT)*, vol. 22, no. 12, pp. 1649–1668, 2012.
- [26] ISO/IEC JTC 1/SC29, "High Efficiency Coding and Media Delivery in Heterogeneous Environments – Part 2: High Efficiency Video Coding. ISO/IEC 23008-2:2017," Tech. Rep., 2017.
- [27] "Jpeg pleno." [Online]. Available: <https://jpeg.org/jpegpleno/>
- [28] R. Yang, F. Mentzer, L. V. Gool, and R. Timofte, "Learning for video compression with hierarchical quality and recurrent enhancement," in *IEEE Int. Conf. on Computer Vision and Pattern Recognition (CVPR)*, 2020.
- [29] —, "Learning for video compression with recurrent auto-encoder and recurrent probability model," *IEEE J. Sel. Topics Signal Process. (JSTSP)*, vol. 15, no. 2, pp. 388–401, 2021.
- [30] R. Yang, L. V. Gool, and R. Timofte, "OpenDVC: An open source implementation of the DVC video compression method," *CoRR*, vol. abs/2006.15862, 2020.
- [31] G. Lu, W. Ouyang, D. Xu, X. Zhang, C. Cai, and Z. Gao, "DVC: An end-to-end deep video compression framework," in *IEEE Int. Conf. on Computer Vision and Pattern Recognition (CVPR)*, 2019, pp. 10998–11007.
- [32] J. Lin, D. Liu, H. Li, and F. Wu, "M-LVC: Multiple frames prediction for learned video compression," in *IEEE Int. Conf. on Computer Vision and Pattern Recognition (CVPR)*, 2020, pp. 3546–3554.
- [33] Z. Hu, Z. Chen, D. Xu, G. Lu, W. Ouyang, and S. Gu, "Improving deep video compression by resolution-adaptive flow coding," in *Eur. Conf. on Computer Vision (ECCV)*, 2020.
- [34] N. Zou, H. Zhang, F. Cricri, H. Tavakoli, J. Lainema, E. Aksu, M. Hannuksela, and E. Rahtu, "End-to-end learning for video frame compression with self-attention," in *IEEE Conf. on Computer Vision and Pattern Recognition Workshop (CVPRW)*, 2020.
- [35] M. Yilmaz and A. M. Tekalp, "End-to-end rate-distortion optimization for bi-directional learned video compression," in *IEEE Int. Conf. on Image Processing (ICIP)*, 2020.
- [36] M. Levoy and P. Hanrahan, "Light field rendering," in *Proc. 23rd Annu. Conf. Comput. Graph. Interact. Techn. (SIGGRAPH)*, 1996, pp. 31–42.
- [37] J. Schonberger and J. Frahm, "Structure-from-motion revisited," in *IEEE Int. Conf. on Computer Vision and Pattern Recognition (CVPR)*, 2016, pp. 4104–4113.
- [38] I. Oseledets, "Tensor-train decomposition," *SIAM Journal on Scientific Computing*, vol. 33, no. 5, pp. 2295–2317, 2011.
- [39] M. Yin, Y. Sui, S. Liao, and B. Yuan, "Towards efficient tensor decomposition-based dnn model compression with optimization framework," in *IEEE Int. Conf. on Computer Vision and Pattern Recognition (CVPR)*, 2021, pp. 10674–10683.
- [40] S. Boyd, N. Parikh, and E. Chu, *Distributed optimization and statistical learning via the alternating direction method of multipliers*. Now Publishers Inc., 2011.
- [41] A. Fan, P. Stock, B. Graham, E. Grave, R. Gribonval, H. Jegou, and A. Joulin, "Training with quantization noise for extreme model compression," *Int. Conf. on Learning Representations (ICLR)*, 2020.
- [42] K. Honauer, O. Johannsen, D. Kondermann, and B. Goldluecke, "A dataset and evaluation methodology for depth estimation on 4D light fields," in *Asian Conf. on Computer Vision (ACCV)*, 2016, pp. 19–34.
- [43] M. Rerabek and T. Ebrahimi, "New light field image dataset," in *Int. Conf. on Quality of Multimedia Experience (QoMEX)*, no. EPFL-CONF-218363, 2016.
- [44] M. Rizkallah, T. Maugey, C. Yaacoub, and C. Guillemot, "Impact of light field compression on focus stack and extended focus images," in *IEEE Eur. Signal Process. Conf. (EUSIPCO)*, 2016, pp. 898–902.
- [45] J. Shi, X. Jiang, and C. Guillemot, "A framework for learning depth from a flexible subset of dense and sparse light field views," *IEEE Trans. Image Process. (TIP)*, vol. 28, no. 12, pp. 5867–5880, Dec 2019.

- [46] V. Sitzmann, J. Martel, A. Bergman, D. Lindell, and G. Wetzstein, "Implicit neural representations with periodic activation functions," in *Advances in Neural Information Processing Systems (NIPS)*, 2020.
- [47] A. Yu, R. Li, M. Tancik, H. Li, R. Ng, and A. Kanazawa, "Plenotrees for real-time rendering of neural radiance fields," in *IEEE Int. Conf. on Computer Vision (ICCV)*, 2021, pp. 5752–5761.
- [48] B. Y. Feng and A. Varshney, "SIGNET: Efficient neural representation for light fields," in *IEEE Int. Conf. on Computer Vision (ICCV)*, 2021, pp. 14 224–14 233.